Dielectric Measurements on Polymeric Materials by Using Superconducting Microwave Resonators

WOLFGANG MEYER

Abstract—**This paper deals with the theoretical and practical investigation of a test method using superconducting cavity and helical resonators in an oscillator loop, which allows precision measurements to be performed on solid dielectrics in the range of 0.1–10 GHz, and below 9 K. The underlying formulas are an extension of the well-known perturbation formalism and are not restricted to low temperatures. Our experiments resulted in unloaded quality factors of $Q = 5 \cdot 10^7$, between 0.2 and 10 GHz, with a maximum Q (2.2 K, 0.19 GHz) of $9 \cdot 10^8$, which enabled us to observe the smallest loss tangent so far: tan δ (2.2 K, 6.5 GHz) = (3.7 ∓ 5 percent) $\cdot 10^{-7}$ in polyethylene.**

I. Introduction

In connection with recent applications of RF superconductivity (e.g., in the generation and distribution of microwave high power [1]), the superconducting high-energy linear accelerators and fusion reactors [2], or the superconducting microwave communication systems [3], there is growing need for experimental data on microwave low-temperature dielectric properties of materials. This paper deals with the theoretical and practical investigation of a suitable test method which allows high-precision measurements between 0.1 and 10 GHz and 2 and 9 K, by using superconducting helical and cavity resonators in an oscillator loop. We first present the underlying theory of measurement, an extension of the well-known perturbation formalism; subsequently, we describe the cylindrical E_{010} and E_{011} cavities in detail, theoretically as well as their performances, and end up with some results on loss tangents of polymers which are the lowest ever measured outside the optical frequency region.

II. Theory

When a dielectric specimen is inserted into a RF resonator, both the electric (E) and magnetic (H) field configurations change, and quality factor Q and resonance frequency f are altered. By measuring f and Q of the unperturbed and perturbed resonator, dielectric constant ε_2 and loss tangent $\tan \delta = \varepsilon_2''/\varepsilon_2'$ (where $\varepsilon_2 = \varepsilon_2' - j\varepsilon_2''$) of the specimen can be calculated starting from the exact expression for the complex frequency shift

$$\frac{\omega_2 - \omega_1^*}{\omega_2} = \frac{\int_{V_s} [(\varepsilon_1^* - \varepsilon_2)\varepsilon_0 \boldsymbol{E}_1^* \boldsymbol{E}_2 + (\mu_1^* - \mu_2)\mu_0 \boldsymbol{H}_1^* \boldsymbol{H}_2]\, dV_s}{\int_{V_c} (\varepsilon_1^* \varepsilon_0 \boldsymbol{E}_1^* \boldsymbol{E}_2 + \mu_1^* \mu_0 \boldsymbol{H}_1^* \boldsymbol{H}_2)\, dV_c}. \tag{2.1}$$

Equation (2.1) is derived without any assumptions except that the walls are perfectly conducting [4]. In the numerator the integration is over V_s, the volume of the sample; the subscripts 1 and 2 refer to the empty and partially filled cavity, respectively. The complex frequency shift is related to measurable quantities by [5]

$$\frac{\omega_2 - \omega_1^*}{\omega_2} = \frac{f_2 - f_1}{f_2} + \frac{j}{2}\left(\frac{1}{Q_2} - \frac{1}{Q_1}\right) \tag{2.2}$$

which is valid for $Q_1, Q_2 \gg 1$. These are the general equations to be applied in any specific experiment where the real and imaginary parts of the dielectric constant and permeability are measured in terms of the real and imaginary part of the frequency shift.

In this article we will restrict ourselves on nonmagnetic dielectric materials only, i.e., $\mu_1 = \mu_2 = \mu_0$. When inserting a lossy sample, we may regard this procedure as being divided into two steps, thus splitting the overall frequency shift into a real part due to an ideal lossless dielectric (X, real), and an additional frequency shift, caused by introducing losses ($Y + jZ$, complex).

Under conditions $X \ll 1$, $Y \ll X$, which are equivalent to small real frequency shifts and small imaginary field components $\text{Im}\{E_2\} \simeq \tan \delta \cdot \text{Re}\{E_2\} \ll \text{Re}\{E_2\}$

$$\frac{f_2 - f_1}{f_2} \leq 0.1, \qquad \tan \delta \leq 0.1 \tag{2.3}$$

the imaginary part of the overall frequency shift obtains as

$$Z \simeq \frac{\varepsilon_2'' \int_{V_s} \varepsilon_0 |\boldsymbol{E}_2|^2\, dV_s}{\int_{V_c} (\varepsilon_1' \varepsilon_0 |\boldsymbol{E}_2|^2 + \mu_0 |\boldsymbol{H}_2|^2)\, dV_c + \int_{V_s} \varepsilon_0 (\varepsilon_2' - \varepsilon_1') |\boldsymbol{E}_2|^2\, dV_s} \tag{2.4}$$

which together with (2.2) leads to the desired expression for the loss tangent

$$\tan \delta = \frac{1}{2}\left(\frac{\varepsilon_1'}{\varepsilon_2'} - 1\right) \frac{f_2}{f_2 - f_1}\left(\frac{1}{Q_2} - \frac{1}{Q_1}\right) \cdot K \tag{2.5}$$

Manuscript received May 16, 1977; revised August 19, 1977. An extended version of this paper was presented at the 1977 Microwave Symposium, in San Diego, CA, June 1977.

The author is with the Institut für Hochfrequenztechnik, Technische Universität Braunschweig, Braunschweig, West Germany.

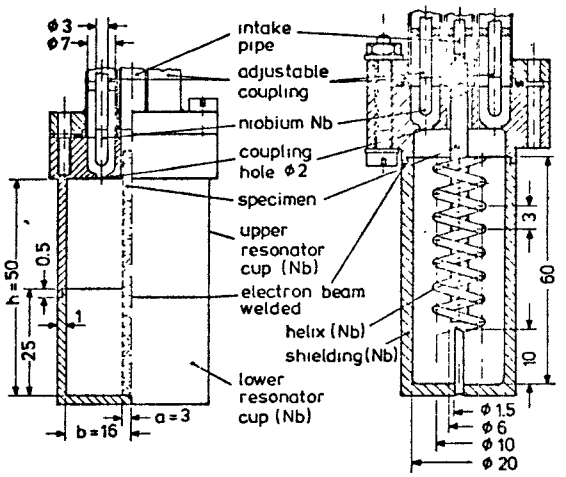

Fig. 1. (a) E_{010} resonator (7 GHz). (b) Helical resonator (0.2–2 GHz).

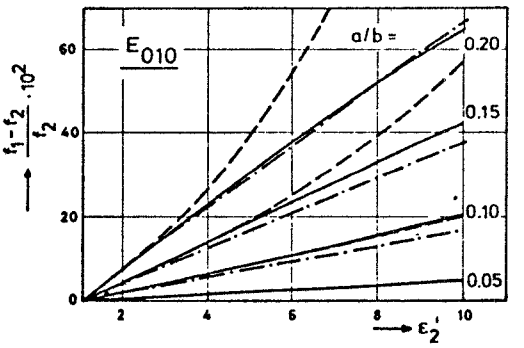

Fig. 2. Frequency shift of cavity (Fig. 1) due to a dielectric ε_2'. Exact equation (4.1): ———. Approximate equation (4.5): —·—·—. Approximate equation (4.7).

where

$$K = \frac{\int_{V_s} \varepsilon_0 \boldsymbol{E}_1 \boldsymbol{E}_2 \, dV_s}{\int_{V_c} (\varepsilon_1' \varepsilon_0 \boldsymbol{E}_1 \boldsymbol{E}_2 + \mu_0 \boldsymbol{H}_1 \boldsymbol{H}_2) \, dV_c} \cdot \left(\varepsilon_2' - \varepsilon_1' + \frac{\int_{V_c} \varepsilon_1' |\boldsymbol{E}_2|^2 \, dV_c}{\int_{V_s} |\boldsymbol{E}_2|^2 \, dV_s}\right). \tag{2.6}$$

The real part of (2.1) equals the real frequency shift, i.e.,

$$\frac{f_2 - f_1}{f_2} = (\varepsilon_1' - \varepsilon_2') \frac{\int_{V_s} \varepsilon_0 \boldsymbol{E}_1 \boldsymbol{E}_2 \, dV_s}{\int_{V_c} (\varepsilon_0 \varepsilon_1' \boldsymbol{E}_1 \boldsymbol{E}_2 + \mu_0 \boldsymbol{H}_1 \boldsymbol{H}_2) \, dV_c}. \tag{2.7}$$

Equations (2.5)–(2.7) represent an extension of the well-known perturbation theory to the lossy case. As the name perturbation implies, the two situations, i.e., the cavity without and with a sample, must be very much alike; this criterion is expressed by condition (2.3). In order to demonstrate the range of application of the above theory and possible simplifications, we will apply the equations above to actual resonators employed at our institute for low-temperature dielectric measurements. The evaluations are restricted to a lossless medium with $\varepsilon_1 = 1$ being initially contained in the cavity, e.g., vacuum, or liquid helium with ε_1 (90 MHz, 4.2 K) = 1.049 and $\tan \delta \leq 10^{-10}$ [6].

III. Microwave Resonators

We use cylindrical cavities at 7 GHz and the helical resonator of Fig. 1 between 0.2 and 2 GHz. Numerical evaluations in this paper are restricted to the cavity resonator, but the same tendencies regarding errors in dielectric constant measurement, etc., can be observed with the helix type.

The cavity is operated in the E_{010} and E_{011} mode, the latter having advantageous wall field configurations which allow the resonator to be made of two identical half-cups without currents flowing across joints and affecting the quality. The analytical field expressions are gained by the exact solution of the boundary value problem outlined in various textbooks on Maxwell's theory. The solutions are given in the Appendix (Sec. A1 and A2), and are referred to subsequently in this paper.

IV. Dielectric Constant Measurement

4.1 Characteristic Equation

With the notations given in Section A2 of the Appendix, the characteristic equation is

$$\frac{k_{2s}}{\varepsilon_2'} \frac{\varepsilon_1'}{k_{2c}} \frac{I_0(k_{2s}a)}{I_1(k_{2s}a)} - \frac{Z_0(k_{2c}a)}{Z_1(k_{2c}a)} = 0. \tag{4.1}$$

The real part of the dielectric constant is readily determined by the numerical calculation of the frequency shift which is introduced in (4.1) as k_{2s},k_{2c}. This evaluation will be referred to as the exact solution.

For small deviations of the transversal phase constants k_{2s},k_{2c} from the empty case k_1

$$k_{2c} = k_1 + \Delta k_2$$
$$k_{2s} = \sqrt{\varepsilon_2'} \cdot (k_1 + \Delta k_2) \tag{4.2}$$

the following simple expression evolves from (4.1):

$$\frac{k_{2s}}{k_{2c}\varepsilon_2'} \frac{2b}{\sqrt{\varepsilon_2'} x_{01} a} \simeq \frac{N_0(x_{01}) + I_1(x_{01}) N_0(x_{01}a/b) \, \Delta k_2 b}{N_0(x_{01}) x_{01} a/(2b) - I_1(x_{01}) \, \Delta k_2 b \cdot 2b/(\pi a x_{01})} \tag{4.3}$$

which is further simplified by using first order approximations of Bessel functions [7]

$$\frac{\Delta k_2}{k_1} \simeq \frac{\pi}{4} \frac{N_0(x_{01})}{I_0(x_{01})} x_{01} \left(\frac{a}{b}\right)^2 (1 - \varepsilon_2'). \tag{4.4}$$

The resultant frequency shift due to the insertion of a dielectric ε_2'

$$\frac{f_2 - f_1}{f_2} \simeq \frac{1.86(a/b)^2(1 - \varepsilon_2')}{1 + 1.86(a/b)^2(1 - \varepsilon_2')} \tag{4.5}$$

is compared with the exact solution for the E_{010} and E_{011} resonators in Figs. 2 and 3, showing reasonable coincidence for small ε-values.

4.2 Cavity Perturbation Formula

Equation (2.7) is of more general interest than the characteristic equation which often is not known in case of more complex sample and cavity geometries. The fields in the (small) specimen are usually the solutions of static problems [5]. For long samples placed in a parallel electrical field, the perturbed field in the interior of the cylinder equals the unperturbed field. With the identity $\boldsymbol{E}_1 \equiv \boldsymbol{E}_2$, (2.2) results in the well-known perturbation formula

$$\frac{f_2 - f_1}{f_2} = \frac{1 - \varepsilon_2'}{2} \frac{\int_{V_s} |\boldsymbol{E}_1|^2 \, dV_s}{\int_{V_c} |\boldsymbol{E}_1|^2 \, dV_c}. \tag{4.6}$$

Its analytical solution with respect to the E_{010} mode ($q = 0$) and the E_{011} mode ($q = 1$—see Sec. A1 of the Appendix) is

$$\frac{f_2 - f_1}{f_2} = \Delta f_2 = \frac{1 - \varepsilon_2'}{2} \cdot \frac{\left\{\frac{(x_{01}a/b)^2}{2}\left[I_0^2\left(x_{01}\frac{a}{b}\right) + I_1^2\left(x_{01}\frac{a}{b}\right)\right] \cdot \left[\left(q\frac{\pi}{h}\right)^2 + (2-q)\left(\frac{x_{01}}{b}\right)^2\right] - \frac{a}{b}x_{01}I_0\left(x_{01}\frac{a}{b}\right) \cdot \left(q\frac{\pi}{h}\right)^2\right\}}{\left\{\frac{x_{01}^2}{2}I_1^2(x_{01})\left[\left(q\frac{\pi}{h}\right)^2 + (2-q)\left(\frac{x_{01}}{b}\right)^2\right]\right\}} \tag{4.7}$$

and is plotted in Figs. 2 and 3, showing the limited range of validity of this often used formula which leads to acceptable results only under very restricted conditions of small dielectric constant and sample dimensions.

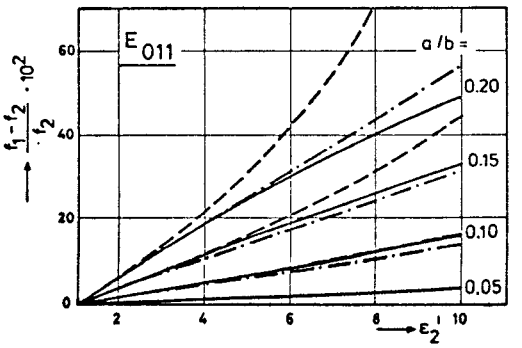

Fig. 3. Frequency shift of cavity (Fig. 1) due to a dielectric ε_2'. Exact equation (4.1): ———. Approximate equation (4.5): — · — · —. Approximate equation (4.7).

The evaluation of the exact equation (2.7) is an elaborate procedure, but it determines the frequency shift very accurately though the transversal phase constants k_{2c}, k_{2s} (or the resonance frequency f_2) included in the field expressions, are not known initially. The frequency shift is stationary against variations of f_2 in the right-hand-side integrals of (2.7), and therefore only needs approximate values to be inserted for k_{2s}, k_{2c}. This is done in Fig. 4 which displays the deviation of the calculated frequency shift according to (2.7), when the frequency f_2 in the field expressions $\boldsymbol{E}_2$ is varied. Departures from the exact shift are ignorable when satisfying the only condition that k_2 must differ from k_1 in the unperturbed state. Fig. 4 was gained by evaluating the following analytical solution of (2.7):

$$\frac{f_2 - f_1}{f_2} = (1 - \varepsilon_2') \frac{[k_z^2 F_1 + k_1 k_{2s}(2-q)F_2]}{[k_z^2 + \varepsilon_2'(2-q)\sqrt{(k_1^2 + k_z^2)(k_{2c}^2 + k_z^2)}F_1 + (k_z^2 + (2-q)\sqrt{(k_1^2 + k_z^2)(k_{2c}^2 + k_z^2)} \cdot F_5 \cdot F_3 \cdot k_{2s}/k_{2c} + k_1 k_{2s}(2-q)(F_2 + F_4 F_5)]}. \tag{4.8}$$

F_1–F_5 denote combinations of Bessel functions, given in Sec. A3 of the Appendix.

4.3 Errors in Dielectric Constant Measurement Due to a Sample Insertion Hole

Equation (2.7) was further employed to compute the influence of a sample insertion hole (Fig. 1) on the resonance frequency and the resulting error in dielectric constant measurement. Equation (2.7) now converts into (4.9) [8], which is an alternative formulation of the resonator action theorem [9]:

$$\frac{f - f_0}{f_0} = \frac{-\varepsilon_2' \int_{V_L} |\boldsymbol{E}_L|^2 \, dV_L}{2 \int_{V_c} |\boldsymbol{E}_1|^2 \, dV_c}. \tag{4.9}$$

The physical interpretation of (4.9) is that for an oscillating electromagnetic system the relative frequency pulling is equal to the relative energy change of the system due to changing its configuration. $\boldsymbol{E}_L$ represents the field configuration inside the infinitely long sample insertion tube of volume V_L (Fig. 1). The circularly symmetric E_{0p} mode in the cavity ensures that only E_{01q} modes will be excited in the tube. We approximate $\boldsymbol{E}_L$ by the E_{01} mode only, because higher order modes are decaying even faster in the below cutoff tube

$$E_{z'L} = \frac{A_L}{j\omega_1 \varepsilon_2'}\left(\frac{x_{01}}{a}\right)^2 I_0\left(\frac{x_{01}}{a}r\right)\exp\left(-\frac{x_{01}}{a}z'\right)$$

$$E_{rL} = \frac{A_L}{\omega_1 \varepsilon_2'}\left(\frac{x_{01}}{a}\right)^2 I_1\left(\frac{x_{01}}{a}r\right)\exp\left(-\frac{x_{01}}{a}z'\right). \tag{4.10}$$

$2'$ is the distance into the tube as measured outward from the interface A between the cavity and the tube (Fig. 5). Following the scopes outlined in [10], we rather arbitrarily equate the integrated square of the unperturbed cavity field at the interface to the integrated square of the tube field at the interface, in order to get the relation between the amplitude factors A_L in (4.10) and A_1 in (A.1) of the Appendix, obtaining

$$A_L = A_1 \frac{a^2 \varepsilon_2}{2b^2 I_1^2(x_{01})}. \tag{4.11}$$

Combining (A.1), (4.10), and (4.11) into (4.9), we arrive at the

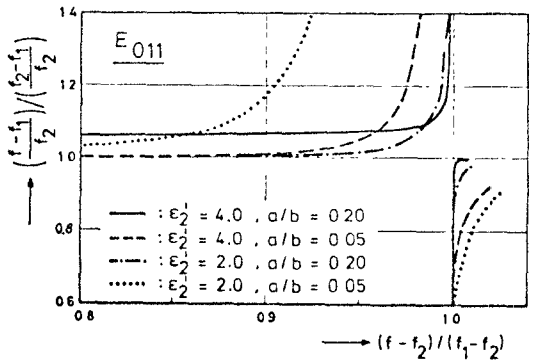

Fig. 4. Solution of (4.8), when f is varied between f_2 and f_1 in the field expressions.

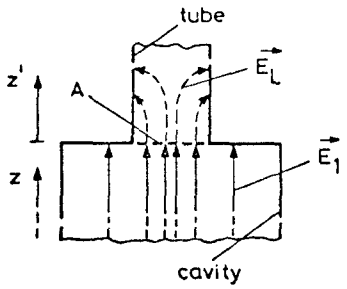

Fig. 5. Electrical field configuration at the sample insertion tube.

following expression for the frequency shift, which is valid for small-hole diameters $2a/2b \leq 0.2$:

$$\frac{f-f_0}{f_0} = \frac{\varepsilon_2' a^3 x_{01}}{2b^4 h I_1^2(x_{01}) \left[\left(\frac{\pi}{h}q\right)^2 + \left(\frac{x_{01}}{b}\right)^2 (2-q)\right]}. \tag{4.12}$$

The error in $\varepsilon_2' - 1$ due to errors in f_1 and f_2 is obtained from the total differentiation of the first order perturbation formula (4.5). With the expression for the errors in frequency, equation (4.12), it finally amounts to

$$\frac{d(\varepsilon_2' - 1)}{\varepsilon_2' - 1} = -\frac{2}{\pi N_0(x_{01}) I_1(x_{01})} \frac{a}{hb^2 \left[\left(\frac{\pi}{h}q\right)^2 + \left(\frac{x_{01}}{b}\right)^2 (2-q)\right]} \frac{f_2}{f_1}. \tag{4.13}$$

Numerical values for frequency shift and error in ε_2' are plotted in Figs. 6 and 7 which show that this effect should not be ignored in high precision measurements.

V. Dissipation Measurement

According to (2.5) the loss tangent depends on the frequency shift as well as on the quality factor Q and field correction factor K. For negligible field distortions $E_1 = E_2$, (2.6) is reduced to

$$K \simeq 1 - 2\,\Delta f_2 \tag{5.1}$$

with Δf_2 denoting the frequency shift according to (4.6).

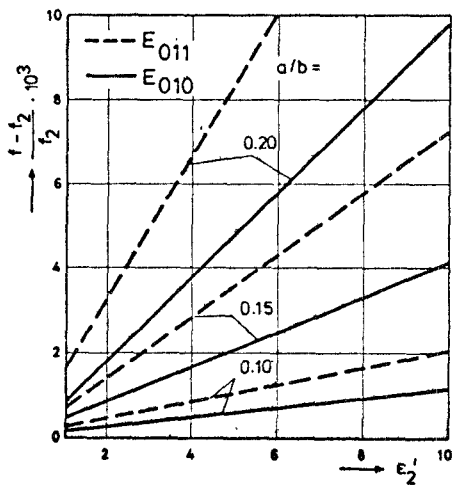

Fig. 6. Change of resonance frequency f_2 due to a sample insertion hole with $2a$ in diameter (eq. (4.12)).

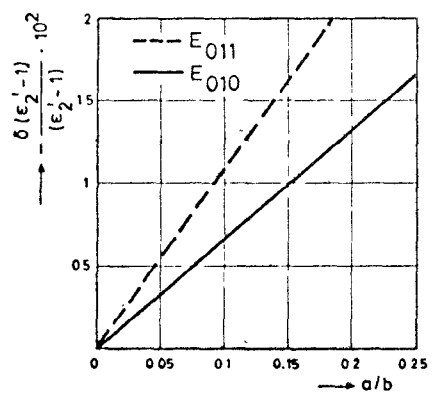

Fig. 7. Relative error of ε_2' measurement due to a sample insertion hole with $2a$ in diameter (eq. (4.13)).

Thus small departures of K from 1 are a quantitative measure of the range of application of the perturbation theory. For the exemplary cavity of Fig. 1, K deviates appreciably from 1, as documented in Fig. 8, and therefore can lead to relative errors in $\tan\delta$—measurement of more than 50 percent if neglected.

Another source of error is the change of the geometric factor G when inserting the specimen. G determines the quality factor Q with the help of the microwave resistance R_A, and depends upon the wall field configuration at the inner surface A of the cavity, i.e., upon the tangential magnetic fields H_{tan}

$$G = Q \cdot R_A = \omega\mu_0 \frac{\int_{V_c} |\boldsymbol{H}|^2 \, dV_c}{\oint_A |\boldsymbol{H}_{tan}|^2 \, dA}. \tag{5.2}$$

Explicit evaluations of (5.2) for the empty $\boldsymbol{H} = \boldsymbol{H}_1$ and perturbed cavity $\boldsymbol{H} = \boldsymbol{H}_2$ result in these analytical expressions for the respective geometric factors

$$G_1 = \sqrt{\frac{\mu_0}{\varepsilon_0}} \cdot \frac{\sqrt{\left(\frac{x_{01}}{b}\right)^2 + \left(q\frac{\pi}{h}\right)^2}}{2\left(\frac{1}{b} + \frac{2}{h}\right)} \tag{5.3}$$

TABLE I
CRITICAL TEMPERATURE T_c, BAND-GAP PARAMETER Δ AND IMPROVEMENT FACTOR V OF MICROWAVE SUPERCONDUCTORS

	Pb	Nb	NbTi	MoRe	Nb_3Sn
$T_c[K]$	7.22	9.25	9.8	10.1	18.2
$\Delta[k_B T_c]$	2.05	1.86	1.73	1.78	2.1
V(4.2 K; 10 GHz)	$5 \cdot 10^2$	$1.4 \cdot 10^3$	$7.5 \cdot 10^3$	$2 \cdot 10^3$	10^4
References	[11], [12]	[11], [12]	[13]	[14]	[15], [16]

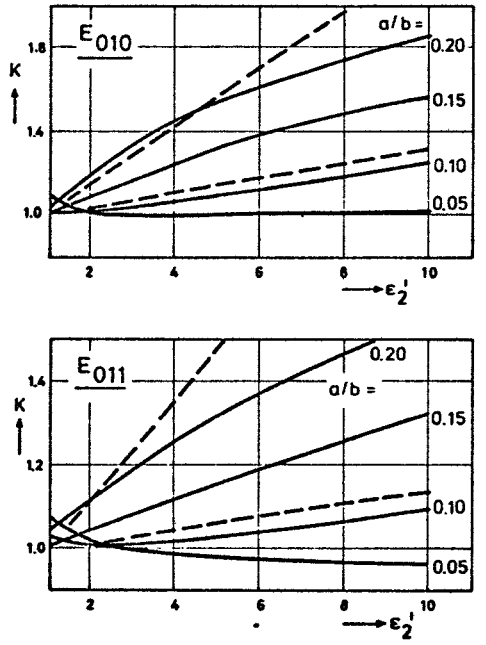

Fig. 8. Correction factor of cavity resonator (Fig. 1). Exact equation (2.6): ———. Approximate equation (5.1): — — —.

$$G_2 = \omega_2 \mu_0 \frac{h}{2}(2-q) \frac{C_1 + \left(\frac{k_{2s}}{k_{2c}} \cdot \frac{F_4}{\varepsilon_2'}\right)^2 C_2}{2C_2 + \left(\frac{k_{2s}}{k_{2c}} \frac{F_4}{\varepsilon_2'}\right)^2 \left[C_2 + Z_1^2(k_{2c}b)\frac{bh}{2}(2-q)\right]}. \quad (5.4)$$

C_1, C_2, F_4, and Z_1 represent combinations of cylinder functions given in the Appendix. Numerical examples for the equivalent change of the Q factor due to modifications of the wall field configuration are displayed in Fig. 9, proving that this effect should be ignored in case of a high enough Q_1 compared to Q_2. Under the same condition the frequency dependence of $R_A(f)$ will be neglected, though it might be strong in superconducting materials.

VI. RF Superconductivity

Measurements of the frequency and temperature dependence of technical superconductors can be split into two contributions to the surface resistance R_A

$$R_A(f,T) = R_{BCS}(f,T) + R_{res}(f). \quad (6.1)$$

Well below the critical temperature T_C and under condition of $hf \leq \Delta/10$ (i.e., for frequencies below 50 GHz), the theoretical BCS surface resistance behaves as

$$R_{BCS} \sim \frac{f^{(1.7 \cdots 2.0)}}{T} \exp\left(-\frac{\Delta}{k_B T_C}\frac{T_C}{T}\right). \quad (6.2)$$

T_C and band-gap parameter Δ for relevant RF superconductors are compiled in Table I.

The table in addition contains the improvement factor V(4.2 K, 10 GHz), which relates the surface resistance of the superconductor (SC) at low temperature to Copper (Cu) at room temperature

$$V(T,f) = R_A(\text{Cu, 300 K}, f)/R_A(\text{SC}, T, f). \quad (6.3)$$

Besides R_{BCS} there appears a residual resistance R_{res} in (6.1), which is practically independent from temperature and is closely related to the state of the surface (smoothness, contaminations, etc.). In many cases, especially at low temperatures < 4.2 K, the lowest surface resistance obtainable is determined by R_{res}, while even lower values could be reached in an ideal superconductor. The physical origin of the residual resistance was not quite understood until now; the most feasible microscopic model is based on phonon exchange among traps in the surface layer of the metal and explains most features of R_{res} (field and frequency dependences) qualitatively [17]–[19].

The available data on the measured BCS resistance is compiled in Fig. 10. Fig. 11 contains the values of R_{res} which were obtained with different, sometimes sophisticated, surface preparation methods, as there are chemical and electrochemical polishing, as well as heating processes. The straight line interpolates our own measurements for Nb, which after machining was first treated chemically in a HF/HNO_3 solution, then electron beam welded and recrystallized at 1300°C in an ultra-high vacuum (UHV). These resonators show unloaded Q's of typically $5 \cdot 10^7$ at 4.2 K in the gigahertz region, with $9 \cdot 10^8$ (at 2.2 K and 0.19 GHz) in excess, which corresponds to an absolute accuracy of tan δ measurement of better than 10^{-7}.

VII. Experimental Procedure and Results

The quantities of (2.5) are resonance frequency, loaded quality factor, and coupling coefficients, which are obtained in a high precision test assembly (described in detail else-

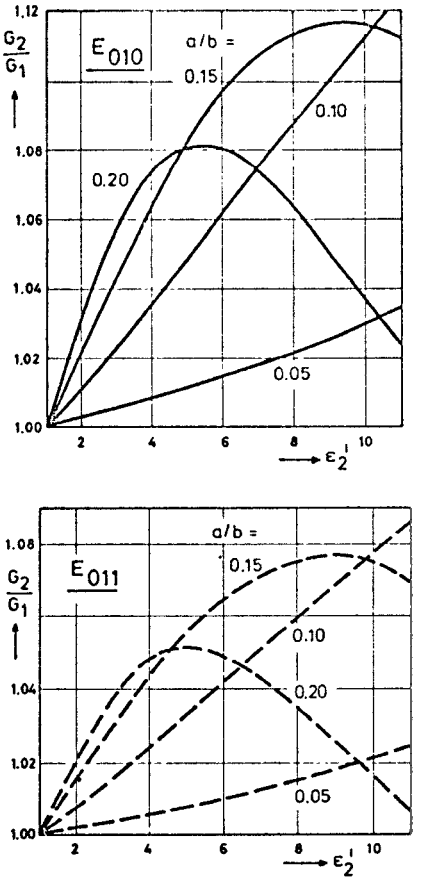

Fig. 9. Change of geometric factor G_2 (eq. (5.4)) due to the insertion of dielectric ε_2'.

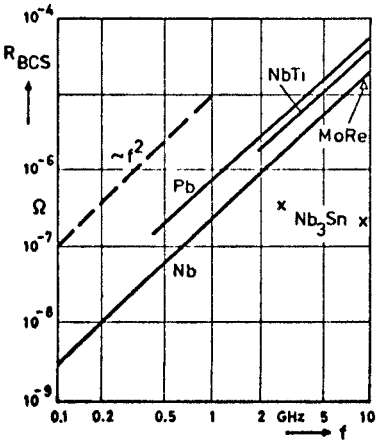

Fig. 10. BCS surface resistance R_{BCS} of microwave superconductors (experimental data partly taken from [12]–[16]).

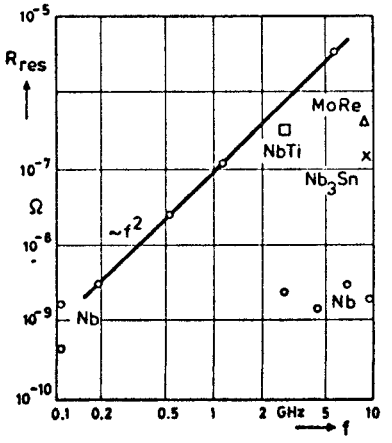

Fig. 11. Residual surface resistance R_{res} of microwave superconductors (experimental data partly taken from [2], [12]–[16]).

where [20]). It consists of the transmission type resonator, which is the frequency determining element in a closed loop, in series with a phase shifter, a transistor amplifier or TWTA, and a p-i-n modulator which interrupts the stationary oscillation which is possible under appropriate phase conditions and sufficient amplification. The quality factor is obtained from the exponential decay of the resonator power envelope. The coupling factors are determined by measuring the incident and transmitted powers during steady state, and the resonance frequency is measured with a microwave counter. Measurement errors do not exceed ∓ 2 percent for Q's greater than 10^4; thus the relative error of tan δ measurement generally amounts to less than 5 percent for tan $\delta \geq 5 \cdot 10^{-7}$. Extensive investigations on various polymers and glasses using this measurement equipment have been published elsewhere [21]–[25] and go beyond the scope of this paper. Briefly summarized, the absorption is enhanced by the dipolarity of the substance, i.e., by impurities or irregularity of the (amorphous) material. Above 10 GHz the loss is mainly due to the low-frequency tail of the infrared absorption peaks extending into the microwave region by many phonon processes, whereas below 1 GHz, losses are mainly caused by phonon-induced tunneling relaxation of impurities or side group dipoles. These molecular processes seem to delimit the intrinsic loss of any polymeric or amorphous material to at least tan $\delta \geq 10^{-7}$. Our smallest measured loss tangent in medium density polyethylene of tan δ (2.2 K, 6.5 GHz) = (3.7 $\mp$ 5 percent) $\cdot 10^{-7}$ approaches this value quite closely.

Acknowledgment

The author wishes to thank Prof. H. G. Unger for suggesting this work; Dr. J. Halbritter, Dr. W. Hoyer, and Dr. P. Kneisel for valuable discussions and various aids; E. Löser for evaluating integral solutions; and the Deutsche Forschungsgemeinschaft for financial support.

Appendix

A1. Field Expressions of the Lowest Eigenmodes in Cylindrical Cavities with Height h and 2b in Diameter

The equations are as follows for $0 \leq r \leq b$:

$$E_{r1} = \frac{A_1}{j\omega_1 \varepsilon_1'} k_1 k_2 I_1(k_1 r) \sin(k_z z)$$

$$E_{z1} = \frac{A_1}{j\omega_1 \varepsilon_1'} k_1^2 I_0(k_1 r) \cos(k_z z)$$

$$H_{\phi 1} = A_1 k_1 I_1(k_1 r) \cos(k_z z) \qquad \text{(A.1)}$$

and the separation condition appears as

$$\omega_1^2 \mu_0 \varepsilon_1' \doteq k_1^2 + k_z^2, \qquad k_1 = x_{01}/b$$

$$k_z = q\frac{\pi}{h}, \qquad x_{01} \equiv 2.405. \tag{A.2}$$

In the above equations $q = 0$ refers to the E_{010} mode, whereas $q = 1$ is to be used in case of the E_{011} resonance. I_0 and I_1 are Bessel functions of the first kind of the order zero and one. A_1 is the amplitude factor dependent upon the energy content of the cavity.

A2. Field Expressions of the Lowest Eigenmodes in a Cylindrical Cavity Containing a Dielectric Sample ε_2' with 2a in Diameter (Fig. 1)

The equations are as follows for $0 \le r \le a$:

$$E_{r2s} = \frac{A_2}{j\omega_2 \varepsilon_2'} k_{2s} k_z I_1(k_{2s} r) \sin(k_z z)$$

$$E_{z2s} = \frac{A_2}{j\omega_2 \varepsilon_2'} k_{2s}^2 I_0(k_{2s} r) \cos(k_z z)$$

$$H_{\phi 2s} = A_2 k_{2s} I_1(k_{2s} r) \cos(k_z z)$$

and $a \le r \le b$:

$$E_{r2c} = \frac{B_2}{j\omega_2 \varepsilon_1'} k_{2c} k_z Z_1(k_{2c} r) \sin(k_z z)$$

$$E_{z2c} = \frac{B_2}{j\omega_2 \varepsilon_1'} k_{2c}^2 Z_0(k_{2c} r) \cos(k_z z)$$

$$H_{\phi 2c} = B_2 k_{2c} Z_1(k_{2c} r) \cos(k_z z). \tag{A.3}$$

$$Z_0(k_{2c} r) = N_0(k_{2c} b) I_0(k_{2c} r) - I_0(k_{2c} b) N_0(k_{2c} r)$$

$$Z_1(k_{2c} r) = N_0(k_{2c} b) I_1(k_{2c} r) - I_0(k_{2c} b) N_1(k_{2c} r). \tag{A.4}$$

The amplitude factors are related by

$$\frac{A_2}{\varepsilon_2'} k_{2s}^2 I_0(k_{2s} a) = \frac{B_2}{\varepsilon_1'} k_{2c}^2 Z_0(k_{2c} a) \tag{A.5}$$

and the separation conditions appear as

$$\omega_2^2 \mu_0 \varepsilon_2' = k_{2s}^2 + k_z^2$$

$$\omega_2^2 \mu_0 \varepsilon_1' = k_{2c}^2 + k_z^2, \qquad k_z = q\frac{\pi}{h}. \tag{A.6}$$

A3. The Solution of Field Integrals (2.7)

The field integrals incorporated in (2.7) are of the form

$$\int r L_0(r) M_0(r)\, dr = \frac{r^2}{2}(L_0 M_0 + L_1 M_1) \tag{A.7}$$

$$\int r L_1(r) M_1(r)\, dr = \frac{r^2}{2}(L_0 M_0 + L_1 M_1) - r L_0 M_1 \tag{A.8}$$

L_n and M_n being arbitrary normal cylinder functions of the order n. The actual solutions of (2.7) yield these results which are to be inserted into (4.8)

$$F_1 = \frac{1}{k_{2s}^2 - k_1^2}[k_1 a I_0(k_1 a) I_1(k_{2s} a) - k_{2s} a I_1(k_1 a) I_0(k_{2s} a)]$$

$$F_2 = \frac{1}{k_1^2 - k_{2s}^2}[k_1 a I_1(k_1 a) I_0(k_{2s} a) - k_{2s} a I_0(k_1 a) I_1(k_{2s} a)]$$

$$F_3 = \frac{1}{k_{2c}^2 - k_1^2}\{N_0(k_{2c} b) \cdot [-k_{2c} b I_1(k_1 b) I_0(k_{2c} b) - k_1 a I_0(k_1 a) I_1(k_{2c} a) + k_{2c} a I_1(k_1 a) I_0(k_{2c} a)]$$

$$- I_0(k_{2c} b)[-k_{2c} b I_1(k_1 b) N_0(k_{2c} b) - k_1 a I_0(k_1 a) N_1(k_{2c} a) + k_{2c} a I_1(k_1 a) N_0(k_{2c} a)]\}$$

$$F_4 = \frac{1}{k_1^2 - k_{2c}^2}\{N_0(k_{2c} b)[k_1 b I_1(k_1 b) I_0(k_{2c} b) - k_1 a I_1(k_1 a) I_0(k_{2c} a) + k_{2c} a I_0(k_1 a) I_1(k_{2c} a)]$$

$$- I_0(k_{2c} b) \cdot [k_1 b I_1(k_1 b) N_0(k_{2c} b) - k_1 a I_1(k_1 a) N_0(k_{2c} a) + k_{2c} a I_0(k_1 a) N_1(k_{2c} a)]\}$$

$$F_5 = \frac{I_0(k_{2s} a)}{Z_0(k_{2c} a)} = \frac{I_0(k_{2s} a)}{N_0(k_{2c} b) I_0(k_{2c} a) - I_0(k_{2c} b) N_0(k_{2c} a)}. \tag{A.9}$$

The subscripts s and c refer to the sample and cavity volume, respectively. Z_0 and Z_1 denote combinations of Bessel functions of the first kind (I_0,I_1) and second kind (N_0,N_1—Neumann functions)

A4. Analytical Evaluation of the Geometric Factor (5.3)

Combining (A.3) with (5.2), integrals are created similar to (A.7) and (A.8). The analytical solution leads to these expressions which are to be inserted into (5.4)

$$C_1 = \frac{a^2}{2}\left(I_0^2(k_{2s}a) + I_1^2(k_{2s}a)\right) - \frac{a}{k_{2s}} I_0(k_{2s}a)I_1(k_{2s}a)$$

$$\begin{aligned} C_2 = {} & N_0^2(k_{2c}b)\left[\frac{b^2}{2}\left(I_0^2(k_{2c}b) + I_1^2(k_{2c}b)\right) - \frac{b}{k_{2c}} I_0(k_{2c}b)I_1(k_{2c}b)\right. \\ & \left. - \frac{a^2}{2}\left(I_0^2(k_{2c}a) + I_1^2(k_{2c}a)\right) + \frac{a}{k_{2c}} I_0(k_{2c}a)I_1(k_{2c}a)\right] \\ & + I_0^2(k_{2c}b)\left[\frac{b^2}{2}\left(N_0^2(k_{2c}b) + N_1^2(k_{2c}b)\right) - \frac{b}{k_{2c}} N_0(k_{2c}b)N_1(k_{2c}b)\right. \\ & \left. - \frac{a^2}{2}\left(N_0^2(k_{2c}a) + N_1^2(k_{2c}a)\right) + \frac{a}{k_{2c}} N_0(k_{2c}a)N_1(k_{2c}a)\right] \\ & - 2I_0(k_{2c}b)N_0(k_{2c}b)\left[\frac{b^2}{2}\left(I_0(k_{2c}b)N_0(k_{2c}b) + I_1(k_{2c}b)N_1(k_{2c}b)\right)\right. \\ & - \frac{b}{k_{2c}} I_0(k_{2c}b)N_1(k_{2c}b) - \frac{a^2}{2}\left(I_0(k_{2c}a)N_0(k_{2c}a) + I_1(k_{2c}a)N_1(k_{2c}a)\right) \\ & \left. + \frac{a}{k_{2c}} I_0(k_{2c}a)N_1(k_{2c}a)\right]. \end{aligned} \tag{A.10}$$

REFERENCES

[1] W. Meyer, "Superconducting microwave power generation and transmission," *Microwave Power Symp. 1976*, Leuven, Belgium, July 27–30, 1976.

[2] H. Pfister, "Superconducting cavities," *Cryogenics*, vol. 16, pp. 17–24, 1976.

[3] K. Mikoshiba *et al.*, "Superconducting coaxial cable as a communication medium with enormous capacity," *IEEE Trans. Commun.*, pp. 874–880, 1976.

[4] E. G. Spencer *et al.*, "Note on cavity perturbation theory," *J. Appl. Phys.*, vol. 23, pp. 130–132, 1957.

[5] M. Sucher and J. Fox, *Handbook of Microwave Measurements II.* New York, 1963.

[6] K. Mittag *et al.*, "Measurements of loss tangents of dielectric materials at low temperatures," IEKP, note 121, Kernforschungszentrum Karlsruhe, Germany, 1973.

[7] M. Abramowitz and I. A. Stegun, *Handbook of Mathematical Functions.* New York, 1965.

[8] H. G. Unger, *Elektromagnetische Wellen II.* Braunschweig, Germany, 1967.

[9] W. R. MacLean, "The resonator action theorem," *Quart. Appl. Math.*, vol. 2, pp. 329–335, 1945.

[10] A. J. Estin and H. E. Bussey, "Errors in dielectric measurements due to a sample insertion hole in a cavity," *IRE Trans. Microwave Theory Tech.*, vol. 8, pp. 650–653, 1960.

[11] E. Voges and K. Petermann, "Losses in superconducting coaxial transmission lines," *Arch. Elek. Übertragung*, vol. AEÜ-27, pp. 384–388, 1973.

[12] J. Halbritter, "Comparison between measured and calculated RF-losses in the superconducting state," *Z. Phys.*, vol. 238, pp. 466–476, 1970.

[13] S. Giordano *et al.*, "Investigation of microwave properties of superconducting $Nb_{0.4}Ti_{0.6}$," *IEEE Trans. Magn.*, vol. 11, pp. 437–440, 1975.

[14] K. Agyeman *et al.*, "Superconducting $M_{0.75}Re_{0.25}$-cavities with high microwave qualities," *IEEE Trans. Magn.*, vol. 13, pp. 343–345, 1977.

[15] B. Hillenbrand *et al.*, "Superconducting Nb_3 Sn-cavities with high microwave qualities," *IEEE Trans. Magn.*, vol. 13, pp. 491–495, 1977.

[16] P. Kneisel, D. Stoltz, and J. Halbritter, "Nb_3 Sn for superconducting RF-cavities," *Adv. Cryogenic Eng.*, vol. 22, pp. 341–346, 1977.

[17] J. Halbritter, "On interfacial tunneling of superconducting surfaces," *Phys. Lett.*, vol. 43A, pp. 309–310, 1973.

[18] ——, "On rf-residual losses and phonon generation," *IEEE Trans. Magn.*, vol. 11, pp. 427–430, 1975.

[19] ——, "On losses caused in rf-cavities by longitudinal electric fields," Ext. Rep. 1/76-1, Inst. Exp. Kernphysik, Kernforschungszentrum Karlsruhe, Germany, 1976.

[20] W. Meyer, "High sensitivity dielectric loss measurements by using superconducting microwave resonators in an oscillator loop," *Electron. Lett.*, vol. 13, pp. 7–8, 1977.

[21] ——, "Dielectric properties of polymeric materials at low temperature and high frequencies," *Proc. 6th Int. Cryogenic Eng. Conf.*, Grenoble, France, May 11–14, 1976, pp. 367–371.

[22] ——, "Cryogenic tunneling losses at microwave frequencies in polymeric dielectrics," *Solid State Commun.*, vol. 22, pp. 285–288, 1977.

[23] G. Frossati, J. Gilchrist, J. C. Lasjaunias, and W. Meyer, "Spectrum of low energy dipolar tunneling states in OH-doped vitreous silica," *J. Phys.*, vol. C-10, pp. L515–L519, 1977.

[24] J. Gilchrist and W. Meyer, "Dielectric loss spectrum of hydrated vitreous silica," *1977 Int. Cryogenic Materials Conf.*, Boulder, CO, Aug. 2–5, 1977.

[25] W. Meyer, "Dielectric loss mechanisms in polymeric solids," *1977 Int. Cryogenic Materials Conf.*, Boulder, CO, Aug. 2–5, 1977.